Conference on Modelling Fluid Flow (CMFF'25)
The 19th International Conference on Fluid Flow Technologies
Budapest, Hungary, August 26-August 29, 2025

COMBINING THE PARTIALLY STIRRED REACTOR WITH A DEM DESCRIPTION: THE PYROLYSIS OF BIOMASS

Davide MAPELLI[1], Don Dasun ATTANAYAKE[1], Berend VAN WACHEM[1], Fabian SEWERIN[1,*]

[1] Chair of Mechanical Process Engineering, Otto-von-Guericke-Universität Magdeburg, Universitätsplatz 2, 39106 Magdeburg, Germany
* Corresponding Author. E-mail: fabian.sewerin@ovgu.de

ABSTRACT

In DEM-CFD descriptions of granular assemblies, the thermochemical state of the interstitial gas is commonly assumed to vary on length scales that are comparable to the supplied spatial resolution. Since chemical reactions, gas-particle mass and heat exchanges and mixing limitations may, however, cause the gas composition to vary on much smaller scales, we present an amendment of the DEM-CFD formulation that is, conceptually, based on the likelihood for a particular gas composition to occur inside a CFD cell. Focussing on a single variable-size control volume at constant pressure, this probabilistic formulation leads to the notion of a partially stirred reactor (PaSR) that interacts with an assembly of DEM particles. The biomass particles we consider here feature a spherical porous structure and are enclosed by passive boundary layers that control the transfer of mass and heat towards the surrounding PaSR-atmosphere. For a fixed particle size, the species mass and gas-solid enthalpy balances representing intra-particle conversion and transport are discretised along the radial coordinate with a standard finite volume approach. The combined DEM-PaSR model can be solved using a statistical approach and, upon incorporation of solid and gas phase reaction mechanisms, provides a test bed for gauging the influence of small-scale thermochemical heterogeneity on the efficacy of the pyrolysis process.

Keywords: Biomass pyrolysis, Discrete element method, Partially stirred reactor, PDF method

ABBREVIATIONS

CFD	Computational fluid dynamics
DEM	Discrete element method
PaSR	Partially stirred reactor
PDF	Probability density function
SDE	Stochastic differential equation

1. INTRODUCTION

In the unresolved DEM-CFD approach for modelling of reactive granular assemblies, the flow field and the composition of the interstitial gas are described on length scales that exceed the particles' sizes. This is achieved with the aid of a spatial filtering operation that eliminates small-scale structures from the flow and composition fields, while referring the presence of particles and gas-particle boundaries to a void fraction and a surface density, respectively. Here, every spatial location is associated with a mean flow and a mean composition that are defined as weighted averages of the interstitial fields over the filter volume centred at the location. In the present article, our objective is to amend the unresolved DEM-CFD formulation by a description of small-scale variability in the gas phase composition as caused by intricate flow structures, thin reaction fronts, particle heating or mass transfer. The incorporation of small-scale compositional heterogeneity not only permits a closed-form treatment of gas phase chemical reactions, but also provides a pathway for including gas-particle mass and heat exchanges with a closure assumption that is less stringent than present hypotheses.

The gas phase composition is commonly expressed in terms of reactive scalars that uniquely define the gas' thermochemical state at low Mach numbers. Drawing on probabilistic methods that originated in the field of turbulent reacting flows [1, 2, 3], the values of the reactive scalars at any location inside the filter volume are conceived of as random variables and associated with a PDF [4]. Starting from the scalars' balance laws on the inter-particle void space and incorporating gas-particle mass and heat exchanges, we obtain an evolution equation for the one-point, one-time joint scalar PDF in which the effects of gas phase chemistry are naturally closed. Since spatial transport involves both two-point statistics and scalar-velocity correlations which cannot be evaluated based on the joint scalar

PDF, the transport terms in the PDF equation require phenomenological closure. For example, species diffusion and heat conduction promote a homogenisation on the smallest scales that is covered by a micromixing model. Additionally, small-scale advection causes reorganisations of the scalars' spatial distributions and is, in the presence of turbulence, often likened to large-scale diffusion. Finally, the incorporation of particles is rendered difficult by the presence of scalar-geometry correlations as well as the distinction between the scalars' distributions along the particle surfaces and their volume distribution. However, if the fluid elements are, at least conceptually, separated from the particle surface by a resistive boundary layer that controls the gas-particle mass and heat transfer, then it may be admissible to approximate the surface distributions in terms of the volume-related joint scalar PDF, a simplification we adopt here.

In the case of large-scale homogeneity, the PDF formulation reduces to the law of a PaSR [5]. This is a model flow system that may be viewed as a constant pressure, variable-volume vessel whose contained fluid elements differ in terms of their thermochemical composition. Physically, the compositional heterogeneity is driven by gas phase chemistry, inflow and outflow, while diffusion-induced micromixing acts in a converse way. In our case, the gas inside the PaSR additionally interacts with an assembly of spherical porous biomass particles through mass and heat transfer rates that are obtained from a passive boundary layer model. The chemical decomposition of the particles' solid skeleton is thermally activated and entails mass effluxes that yield pyrolysis gas and condensed phase oil as main products. The intra-particle transport and conversion are governed by balance laws for the species masses and the combined gas-solid enthalpy. The latter is evaluated based on the assumption that there is no temperature slip between the solid matrix and the intra-particle gas at any radial position. Upon spatial discretisation, the intra-particle balance laws turn into DEM equations that can be integrated in time alongside the PaSR equation.

Albeit idealised, the combined DEM-PaSR formulation we present constitutes a powerful computer-based tool for analysing the influence that the commonly disregarded small-scale variability of the gas composition has on the pyrolysis process. This, in turn, is a first step towards enriching the unresolved DEM-CFD approach by a description of small-scale variability and accommodating gas phase chemistry without intervening assumptions. As reference, Table 1 lists the modelling assumptions and simplifications we introduce in the following on part of the gas phase, the compositional heterogeneity and a single biomass particle.

The present article is organised as follows: After recalling the notion of a spatial filter, the closure challenges associated with small-scale interstitial transport, chemical reactions and gas-particle interactions are indicated and a transport equation for the joint scalar PDF is formulated (Section 2). This equation is coupled to the governing DEM equations through joint scalar statistics that represent the diversity of far-field compositions experienced by the DEM particles. Following a reduction to the PaSR (Section 3), we present a single particle model for biomass alongside the rates at which mass and enthalpy are emitted through a passive boundary layer (Section 4). The relevant numerical solution methods are briefly outlined (Section 5), before we conclude with a summary and an outlook (Section 6).

2. MODELLING FRAMEWORK

A granular assembly is a packed or slowly moving bed of centimetre-sized particles (Figure 1). In pyrolysis reactors, the bed is subjected to a high-temperature treatment by directing a hot inert gas through the bed's void space $\Omega_g(t)$. The interstitial gas behaves as a multicomponent ideal gas and is described in terms of the velocity $\mathbf{u}_g(\mathbf{x},t)$, the pressure $p_g(\mathbf{x},t)$ and the reactive scalars $\mathbf{\Phi} = (\mathbf{Y}_g, h_g)$ that encompass the species mass fractions $\mathbf{Y}_g(\mathbf{x},t) = (Y_{g,k}(\mathbf{x},t))_{k\in\mathcal{G}}$ and the gas enthalpy $h_g(\mathbf{x},t)$. The label set $\mathcal{G}$ that appears here contains the molecular formulas of all gas phase species. If the Mach number is small, then the thermodynamic pressure P is distinct from the mechanical pressure $p_g(\mathbf{x},t)$ and remains uniform across the flow domain. Consequently, the reactive scalars uniquely define the thermal state of the gas and both the gas temperature T and the gas density ρ_g may be computed in terms of $\mathbf{\Phi}$ at $(\mathbf{x},t)$ [6],

$$h_g = \sum_{k\in\mathcal{G}} Y_{g,k} h_k(T), \tag{1}$$

$$\rho_g = \frac{PW_g}{RT}. \tag{2}$$

Here, h_k denotes the specific enthalpy of species $k \in \mathcal{G}$ and R represents the universal gas constant. The gas' mean molecular weight W_g, moreover, is related to the species' molecular weights W_k according to $W_g = 1/\sum_{k\in\mathcal{G}}(Y_k/W_k)$.

On the void space $\Omega_g(t)$, the flow field $(\mathbf{u}_g, p_g)$ is governed by the variable-density Navier-Stokes equations [7, Chapter 1]. In the case of equal diffusivities $D(\mathbf{\Phi})$ and a Lewis number of unity ($Le = 1$), the reactive scalars Φ_k, moreover, obey the transport equations [7, Chapter 1]

$$\frac{\partial\rho_g\Phi_k}{\partial t} + \nabla_{\mathbf{x}}\cdot\left(\rho_g\mathbf{u}_g\Phi_k\right) = \nabla_{\mathbf{x}}\cdot\left(\rho_g D\nabla_{\mathbf{x}}\Phi_k\right) + \rho_g\dot{\omega}_k \tag{3}$$

with $k \in \mathcal{G}' = \mathcal{G}\cup\{h_g\}$. For $k\in\mathcal{G}$, $\dot{\omega}_k(\mathbf{\Phi})$ represents the rate (in $[\mathrm{kg}_k/(\mathrm{kg(g)\,s})]$) at which gas phase chemical reactions cause a species to form or vanish. The gas enthalpy, by contrast, is a conserved scalar and its associated source term $\dot{\omega}_{h_g}$ vanishes. Based on a Schmidt number Sc of 0.7, the common diffusivity $D(\mathbf{\Phi})$ in Eq. (3) is evaluated in terms

Table 1. Summary of the modelling assumptions we introduce in Sections 2 to 4. The properties of the gas phase listed in the first column also apply to the gas in the pore space and the boundary layer of a particle.

Gas phase	PDF formulation	Particle model
• Ideal gas law (Eq. (2)) • Equal diffusivities ($Sc = 0.7$) • $Le = 1$ • Low Mach number	• IEM model • $f_p^\rho = f^\rho$ • Large-scale homogeneity (PaSR)	• Spherical symmetry • Constant particle volume • No internal gas-solid temperature slip • Isolated and quasi-steady boundary layers with conductivities based on surface/far-field scalars • No gas phase chemistry

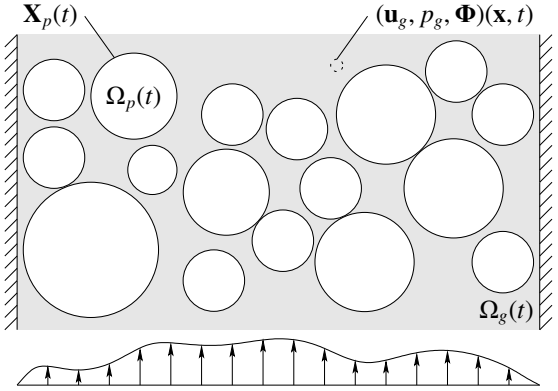

Figure 1. Illustration of a two-dimensional cut through a packed bed of spherical particles.

of the viscosity $\mu_g(\mathbf{\Phi})$ [8, Chapter 2] according to $D(\mathbf{\Phi}) = \mu_g(\mathbf{\Phi})/(\rho_g(\mathbf{\Phi})Sc)$ [9].

In order to reduce the spatial resolution requirements on the interstitial fields, Anderson and Jackson [10] introduced a spatial filtering operation based on a non-negative kernel $g(r)$ with $r \geq 0$. In particular, the spatially filtered counterpart $\langle Q(\mathbf{u}_g, \mathbf{\Phi})\rangle(\mathbf{x}, t)$ of an observable $Q(\mathbf{u}_g(\mathbf{x}, t), \mathbf{\Phi}(\mathbf{x}, t))$ on $\Omega_g(t)$ is defined as

$$\begin{aligned}&\varepsilon_g(\mathbf{x}, t)\langle Q(\mathbf{u}_g, \mathbf{\Phi})\rangle(\mathbf{x}, t)\\ &= \int_{\Omega_g(t)} g(\|\mathbf{x} - \mathbf{y}\|) Q(\mathbf{u}_g(\mathbf{y}, t), \mathbf{\Phi}(\mathbf{y}, t))\,\mathrm{d}\mathbf{y},\end{aligned} \tag{4}$$

where $\varepsilon_g(\mathbf{x}, t)$ denotes the void fraction. Within the scope of the unresolved DEM-CFD approach, the characteristic length scale associated with the filter kernel g is chosen much larger than the particles' sizes. Since the advective terms in the filtered continuity equation are naturally closed if the filtered velocity is amended by density-weighting, we further define the density-weighted average

$$\langle Q(\mathbf{u}_g, \mathbf{\Phi})\rangle_\rho = \frac{\langle \rho_g(\mathbf{\Phi}) Q(\mathbf{u}_g, \mathbf{\Phi})\rangle}{\langle \rho_g(\mathbf{\Phi})\rangle}. \tag{5}$$

In a similar way as in Eqs. (4) and (5), the spatial average $\{\cdot\}_p$ along the surface $\partial\Omega_p(t)$ of particle p [11, Chapter 8] and its density-weighted counterpart $\{\cdot\}_p^\rho$ are introduced. Here, the role of ε_g is taken on by the particle surface density $\xi_p = \{1\}_p$. In the following, we additionally employ the variable $\mathbf{X}_p(t)$ to indicate the degrees of freedom that define the current state of particle p.

By applying the filtering operation $\langle\cdot\rangle$ to Eq. (3), substituting the definitions of the density-weighted volume and surface averages and incorporating the mass and enthalpy fluxes $\rho_g(\mathbf{\Phi})\dot{s}_k(\mathbf{\Phi}, \mathbf{X}_p)$ across the particle boundaries, we obtain [3, 12]

$$\begin{aligned}&\frac{\partial \varepsilon_g \langle\rho_g\rangle\langle\Phi_k\rangle_\rho}{\partial t} + \nabla_{\mathbf{x}} \cdot \left(\varepsilon_g \langle\rho_g\rangle\langle\mathbf{u}_g\Phi_k\rangle_\rho\right)\\ &= \nabla_{\mathbf{x}} \cdot \left(\varepsilon_g \langle\rho_g\rangle\langle D\nabla_{\mathbf{x}}\Phi_k\rangle_\rho\right) + \varepsilon_g\langle\rho_g\rangle\langle\dot{\omega}_k\rangle_\rho\\ &\quad + \sum_p \xi_p \{\rho_g\}_p \{\dot{s}_k\}_p^\rho\,.\end{aligned} \tag{6}$$

Apart from the accumulation term on the left hand side of Eq. (6), all transport, reaction and gas-particle transfer processes remain unclosed in terms of $\langle\mathbf{u}_g\rangle_\rho$ and $\langle\mathbf{\Phi}\rangle_\rho$. In particular, the spatial advection and diffusion terms involve $\mathbf{u}_g$-$\mathbf{\Phi}$-correlations and spatial gradients, respectively, whereas the rates $\dot{\boldsymbol{\omega}}$ and $\dot{\mathbf{s}}(\cdot, \mathbf{X}_p)$ are, generally, nonlinear in $\mathbf{\Phi}$ and the gas-particle fluxes involve surface instead of volume averages. Indeed, the filtered fields $\langle\mathbf{u}_g\rangle_\rho$ and $\langle\mathbf{\Phi}\rangle_\rho$ do not include any information on the small-scale interdependency of $\mathbf{u}_g$ and $\mathbf{\Phi}$ or on their spatial distributions inside the filter's support. For the gas phase chemistry, a common closure hypothesis is the assumption of small-scale homogeneity that permits an evaluation of the filtered reaction rates in terms of the filtered composition, $\langle\dot{\boldsymbol{\omega}}(\mathbf{\Phi})\rangle_\rho = \dot{\boldsymbol{\omega}}(\langle\mathbf{\Phi}\rangle_\rho)$ [13]. In the context of unresolved DEM-CFD formulations for reactive granular assemblies, however, this assumption is not met if interstitial reaction fronts develop, mixing limitations persist or heterogeneities in the particles' mass or heat releases occur.

In order to augment the physical description of the interstitial gas by information on the values that the reactive scalars attain throughout the volume of a filter centred at $\mathbf{x}$, we adopt a technique that has originally been developed in the context of turbulent reacting flows [3, 4]. Here, the density-weighted PDF $f^\rho(\boldsymbol{\phi}, \mathbf{x}, t) = \langle\delta(\boldsymbol{\phi} - \mathbf{\Phi})\rangle_\rho(\mathbf{x}, t)$ is considered as a large-scale descriptor of the gas phase composition in place of the filtered scalars $\langle\mathbf{\Phi}\rangle_\rho(\mathbf{x}, t)$. The argument $\boldsymbol{\phi}$ of $f^\rho(\boldsymbol{\phi}, \mathbf{x}, t)$ is referred to as the sample space variable and ranges over all possible composi-

tion vectors. In the absence of density-weighting, the probability $f(\boldsymbol{\phi}, \mathbf{x}, t)\,\mathrm{d}\boldsymbol{\phi}$ with

$$f(\boldsymbol{\phi}, \mathbf{x}, t) = \frac{\langle \rho_g(\boldsymbol{\Phi})\rangle(\mathbf{x}, t) f^\rho(\boldsymbol{\phi}, \mathbf{x}, t)}{\rho_g(\boldsymbol{\phi})} \tag{7}$$

may be interpreted as the fraction of fluid elements near $\mathbf{x}$ that possess a composition $\boldsymbol{\Phi}$ in $[\boldsymbol{\phi}, \boldsymbol{\phi} + \mathrm{d}\boldsymbol{\phi})$. By taking the time derivative of $\varepsilon_g \langle \rho_g \rangle \langle \delta(\boldsymbol{\phi} - \boldsymbol{\Phi}) \rangle_\rho$ and substituting Eq. (3) alongside the mass balance equation and the flux boundary conditions at the particle surfaces, the following evolution equation for f^ρ is obtained,

$$\begin{aligned} &\frac{\partial \varepsilon_g \langle \rho_g \rangle f^\rho}{\partial t} + \nabla_{\mathbf{x}} \cdot \left(\varepsilon_g \langle \rho_g \rangle f^\rho \left\langle \mathbf{u}_g + \frac{\nabla_{\mathbf{x}} (\rho_g D)}{\rho_g} \middle| \boldsymbol{\phi} \right\rangle \right. \\ &\left. + \sum_p \xi_p \{\rho_g\}_p f_p^\rho D(\boldsymbol{\phi}) \{\mathbf{n}|\boldsymbol{\phi}\}_p \right) \\ &= \nabla_{\mathbf{x}} \cdot \left[D(\boldsymbol{\phi}) \nabla_{\mathbf{x}} \left(\varepsilon_g \langle \rho_g \rangle f^\rho \right) \right] \\ &\quad - \nabla_{\boldsymbol{\phi}} \cdot \left(\varepsilon_g \langle \rho_g \rangle f^\rho \dot{\omega}(\boldsymbol{\phi}) \right) + \mathcal{M} f^\rho + \sum_p \mathcal{S}_p f_p^\rho, \end{aligned} \tag{8}$$

where $\mathbf{n}(\mathbf{x}, t)$ denotes the unit normal vector on the surface of a particle and the particle-specific operator $\mathcal{S}_p$ is given by

$$\begin{aligned} \mathcal{S}_p f_p^\rho &= \xi_p \{\rho_g\}_p f_p^\rho \sum_{k \in \mathcal{G}} \dot{s}_k(\boldsymbol{\phi}, \mathbf{X}_p) \\ &- \nabla_{\boldsymbol{\phi}} \cdot \left[\xi_p \{\rho_g\}_p f_p^\rho \left(\dot{\mathbf{s}}(\boldsymbol{\phi}, \mathbf{X}_p) - \boldsymbol{\phi} \sum_{k \in \mathcal{G}} \dot{s}_k(\boldsymbol{\phi}, \mathbf{X}_p) \right) \right]. \end{aligned} \tag{9}$$

In Eq. (8), the influence of gas phase chemistry on the temporal evolution of f^ρ is naturally closed, while the contributions by the particles involve the unknown density-weighted surface PDFs $f_p^\rho(\boldsymbol{\phi}, \mathbf{x}, t) = \{\delta(\boldsymbol{\phi} - \boldsymbol{\Phi})\}_p^\rho(\mathbf{x}, t)$. Because the gas is separated from the particle surface by a boundary layer (Section 4) and since insights into the relation of f_p^ρ and f^ρ are yet absent, we adopt the simplifying closure hypothesis that the PDF f^ρ associated with the filter volume about $\mathbf{x}$ is representative also of the scalars' distribution f_p^ρ along the surface of particle p, $f_p^\rho = f^\rho$. The operator $\mathcal{M}$ in Eq. (8) represents micromixing and reads

$$\begin{aligned} \mathcal{M} f^\rho = -\varepsilon_g \langle \rho_g \rangle \sum_{k,l \in \mathcal{G}'} \frac{\partial^2}{\partial \phi_l \partial \phi_k} \Big(D(\boldsymbol{\phi}) \\ \times f^\rho \langle \nabla_{\mathbf{x}} \Phi_l \cdot \nabla_{\mathbf{x}} \Phi_k | \boldsymbol{\phi} \rangle \Big). \end{aligned} \tag{10}$$

Like the large-scale advection term on the left hand side of Eq. (8), this term involves conditional expectations and, hence, remains unclosed in terms of f^ρ. Since f^ρ does not include any information on the spatial arrangement of the fluid elements throughout the filter volume or on their velocities, neither filtered gradients nor $\mathbf{n}$-$\boldsymbol{\Phi}$- or $\mathbf{u}_g$-$\boldsymbol{\Phi}$-correlations can be evaluated based on f^ρ. On the positive side, f^ρ permits the direct evaluation of filtered $\boldsymbol{\Phi}$-dependent functions. For example, the filtered reaction rates are obtained as

$$\langle \dot{\omega} \rangle = \langle \rho_g \rangle \int \frac{\dot{\omega}}{\rho_g} f^\rho \, \mathrm{d}\boldsymbol{\phi}. \tag{11}$$

In order to close the micromixing contribution $\mathcal{M} f^\rho$ in terms of f^ρ, we employ the IEM (Interaction by Exchange with the Mean) model [5, 9]. This model is based on the idea that f^ρ relaxes towards the perfectly mixed state $\delta(\boldsymbol{\phi} - \langle \boldsymbol{\Phi} \rangle_\rho)$ over the time scale τ_{mix},

$$\mathcal{M} f^\rho = \frac{\varepsilon_g \langle \rho_g \rangle}{\tau_{\mathrm{mix}}} \nabla_{\boldsymbol{\phi}} \cdot \left[\left(\boldsymbol{\phi} - \langle \boldsymbol{\Phi} \rangle_\rho \right) f^\rho \right]. \tag{12}$$

Despite its shortcomings, the IEM model has the merit of conceptual and formal simplicity; it may be admissible if our objective is to assess in a qualitative, indicative way how small-scale heterogeneity affects process-level predictables.

Within the scope of DEM models of granular assemblies, temporal changes in the degrees of freedom $\mathbf{X}_p(t)$ of particle p are brought about by intra-particle conversion as well as momentum, heat and mass exchanges between the particle, the interstitial gas and the neighbouring particles. Excluding direct particle-particle interactions, the evolution laws of the DEM degrees of freedom can often be cast into a system of differential algebraic equations,

$$\mathbf{M}(\mathbf{X}_p(t)) \frac{\mathrm{d}\mathbf{X}_p(t)}{\mathrm{d}t} = \left\langle \dot{\mathbf{h}}(\langle \mathbf{u}_g \rangle|_p, \boldsymbol{\Phi}(t), \mathbf{X}_p(t)) \right\rangle \tag{13}$$

for $p = 1, 2, \ldots$. Here, $\mathbf{M}(\mathbf{X}_p(t))$ is a mass matrix that may be singular, $\langle \mathbf{u}_g \rangle|_p$ represents the filtered gas velocity experienced by particle p and $\dot{\mathbf{h}}(\langle \mathbf{u}_g \rangle|_p, \boldsymbol{\Phi}(t), \mathbf{X}_p(t))$ encompasses the rates associated with intra-particle processes and gas-particle interactions.

In summary, the combined DEM-PDF framework is based on Eq. (13) as well as modelled forms of Eq. (8) and the filtered gas phase momentum equation. Note that the filtered continuity equation follows as a consequence of Eq. (8) and that the filtered gas density $\langle \rho_g \rangle$ may be obtained from f^ρ by substituting unity for $\dot{\omega}$ in Eq. (11) [3],

$$\langle \rho_g \rangle = \left\langle \frac{1}{\rho_g} \right\rangle_\rho^{-1} = \left(\int \frac{f^\rho}{\rho_g} \, \mathrm{d}\boldsymbol{\phi} \right)^{-1}. \tag{14}$$

In order to circumvent the closure challenge associated with large-scale advection while maintaining a detailed description of small-scale compositional heterogeneity, the DEM-PDF approach is simplified to the case of large-scale homogeneity. This reduction gives rise to the concept of a PaSR that exchanges mass and heat with a granular assembly.

3. REDUCTION TO THE PARTIALLY STIRRED REACTOR

The PaSR is a simplified flow model in which the physical descriptors of the reactive gas are assumed to be uniform across the reactor domain (Fig-

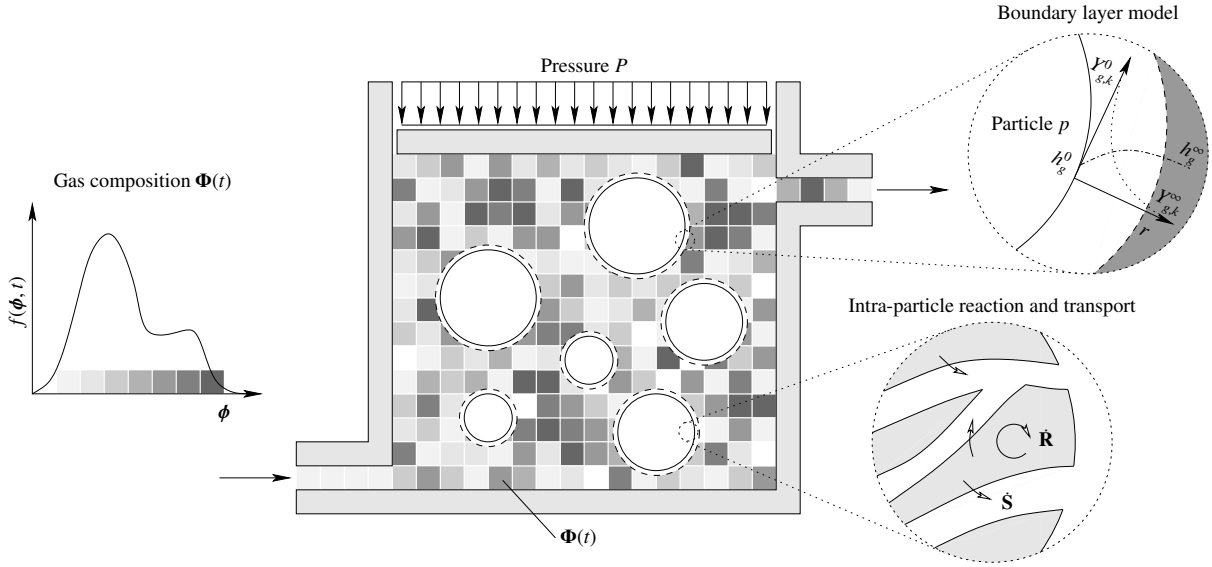

Figure 2. Schematic illustration of a constant pressure PaSR containing an assembly of spherical biomass particles (white disks) with modelled boundary layers (dashed circles). The grey patches indicate individual fluid elements whose thermochemical states $\mathbf{\Phi}(t)$ are distributed according to $f(\cdot, t) = \langle \rho_g(\mathbf{\Phi}) \rangle(t) f^\rho(\cdot, t)/\rho_g(\cdot)$. Note that, in slight departure from the graphical depiction, the fluid elements' individual extents are vanishingly small and that every fluid element inside the PaSR yields a far-field composition $\mathbf{\Phi}(t) = (\mathbf{Y}_g^\infty, h_g^\infty)$ with which a DEM particle interacts.

ure 2). If the thermodynamic pressure P remains constant, then the volume of the reactor changes commensurate with the temporal changes in the mean gas density $\langle \rho_g \rangle$. The distinguishing feature of the PaSR is that the thermochemical composition $\mathbf{\Phi}(t)$ of the gas inside the reactor is a vector-valued random variable with associated PDF $f(\cdot, t) = \langle \rho_g(\mathbf{\Phi}) \rangle(t) f^\rho(\cdot, t)/\rho_g(\cdot)$. If we interpret $\mathbf{\Phi}(t)$ as the composition of a single fluid element chosen uniformly randomly from within the reactor, then the PDF $f(\cdot, t)$ quantifies the compositional variability among the fluid elements. In Figure 2, the fluid elements are depicted as white-bordered squares and the shadings reflect the compositions they carry. While fluid elements are infinitely small, the finite extent of the squares is merely an aid to the graphical illustration. In particular, we emphasise that the white border lines do not correspond to a grid.

From Eqs. (8) and (12), the evolution law governing f^ρ is obtained by integrating over the reactor domain $\Omega(t)$ and substituting the filtered mass balance [5],

$$\begin{aligned} &\frac{\partial f^\rho}{\partial t} + \frac{f^\rho - f_{\text{in}}^\rho}{\tau_{\text{res}}} \\ &= f^\rho \sum_p \frac{\xi_p}{\varepsilon_g} \sum_{k \in \mathcal{G}} \Big(\dot{s}_k(\boldsymbol{\phi}, \mathbf{X}_p) - \langle \dot{s}_k(\mathbf{\Phi}, \mathbf{X}_p) \rangle_\rho \Big) \\ &\quad - \nabla_{\boldsymbol{\phi}} \cdot \Bigg\{ f^\rho \Bigg[\dot{\omega}(\boldsymbol{\phi}) - \frac{1}{\tau_{\text{mix}}} \Big(\boldsymbol{\phi} - \langle \mathbf{\Phi} \rangle_\rho \Big) \\ &\quad + \sum_p \frac{\xi_p}{\varepsilon_g} \Big(\dot{\mathbf{s}}(\boldsymbol{\phi}, \mathbf{X}_p) - \boldsymbol{\phi} \sum_{l \in \mathcal{G}} \dot{s}_l(\boldsymbol{\phi}, \mathbf{X}_p) \Big) \Bigg] \Bigg\}. \end{aligned} \tag{15}$$

Here, τ_{res} represents the mean residence time of the fluid elements inside the reactor and f_{in}^ρ is the joint scalar PDF associated with the gas flowing into the PaSR. In view of our closure assumption $f_p^\rho = f^\rho$, the density-weighted surface mean $\{\dot{s}_k(\mathbf{\Phi}, \mathbf{X}_p)\}_p^\rho$ associated with particle p has been approximated in terms of $\langle \dot{s}_k(\mathbf{\Phi}, \mathbf{X}_p) \rangle_\rho$ in Eq. (15).

Although we turn to a specific particle model in the following, the DEM-PaSR formulation is not restricted to this model (or, indeed, the process of biomass pyrolysis). Formally, the main conditions on the single particle model and the enveloping boundary layer are that the particle's degrees of freedom $\mathbf{X}_p$ obey Eq. (13) and that rate expressions for the mass and enthalpy fluxes $\rho_g(\mathbf{\Phi}) \dot{s}_k(\mathbf{\Phi}, \mathbf{X}_p)$, $k \in \mathcal{G}'$, crossing into the bulk gas are available.

4. MODEL FOR THE CONVERSION OF A BIOMASS PARTICLE

Considering a spherically symmetrical particle, we present a spatially one-dimensional model for the decomposition of biomass that captures both internal heat and mass transfer limitations and the transfer resistance imparted by the boundary layer surrounding the particle. While temperature inhomogeneities in thermally thick biomass particles have been accounted for in past DEM formulations [14, 15, 16], mass transport limitations associated with the gas flow through the particle's pore space or the gas-particle boundary layer have not yet been included to our awareness [17].

Since biomass particles naturally exhibit a complicated porous structure [18], we consider a single

particle with radius R as the union of a solid matrix with porosity $\psi(r,t)$, $r \in [0,R]$, and a pore space gas. As the particle's pyrolysis commences, the intra-particle solid matrix decomposes into solid and gaseous products [19]. The solid products are thought to remain attached to the matrix, while the gas products are released to the immediate pore space and migrate through the pore structure towards the ambient gas. Because of the short intra-particle gas retention times [20], gas phase chemical reactions inside the pore space are omitted. The chemical composition of the solid phase is described in terms of the mass fractions $\mathbf{Y}_s(r,t) = (Y_{s,i}(r,t))_{i\in\mathcal{S}}$ of the solid species whose labels i are aggregated into the set $\mathcal{S}$. Owing to pyrolysis reactions, the mass density of the solid species $i \in \mathcal{S}$ changes in time according to

$$\frac{\partial \rho_s Y_{s,i}}{\partial t} = \dot{R}_i, \tag{16}$$

where ρ_s is the constant mass density of the solid matrix and $\dot{R}_i(\mathbf{Y}_s, T)$ (in $[\mathrm{kg}_i/(\mathrm{s\,m^3(s)})]$) is the net mass production rate of solid species i due to pyrolysis. Since we assume the combined gas-solid volume of the particle to remain unchanged during its conversion, the porosity ψ changes only as a consequence of the production or consumption of the solid species' masses,

$$\frac{\partial \psi}{\partial t} = -\frac{(1-\psi)}{\rho_s}\sum_{i\in\mathcal{S}} \dot{R}_i. \tag{17}$$

Similar to the gas in the inter-particle void space of a particle assembly, the chemical make-up of the gas inside the particle's pore space is determined by the species mass fractions $\mathbf{Y}_g(r,t)$. Denoting by $\dot{S}_k(\mathbf{Y}_s, T)$ (in $[\mathrm{kg}_k/(\mathrm{s\,m^3(s)})]$) the rate at which species $k \in \mathcal{G}$ is released during the solid matrix's decomposition, the species-specific mass balance reads in spherical coordinates

$$\begin{aligned}&\frac{\partial \rho_g \psi Y_{g,k}}{\partial t} + \frac{1}{r^2}\frac{\partial}{\partial r}\left(r^2 \rho_g \psi u_g Y_{g,k}\right)\\ &= \frac{1}{r^2}\frac{\partial}{\partial r}\left(r^2 \rho_g \psi D \frac{\partial Y_{g,k}}{\partial r}\right) + (1-\psi)\dot{S}_k,\end{aligned} \tag{18}$$

where $u_g(r,t)$ represents the radial gas velocity. Upon summation over all species $k \in \mathcal{G}$, Eq. (18) yields the local mass balance

$$\frac{\partial \rho_g \psi}{\partial t} + \frac{1}{r^2}\frac{\partial}{\partial r}\left(r^2 \rho_g \psi u_g\right) = (1-\psi)\sum_{k\in\mathcal{G}} \dot{S}_k. \tag{19}$$

At every radial location, the solid matrix and the gas inside the particle's pore space are assumed to be thermally equilibrated. Consequently, the joint gas-solid enthalpy balance is given by [21]

$$\begin{aligned}&\frac{\partial \rho h}{\partial t} + \frac{1}{r^2}\frac{\partial}{\partial r}\left(r^2 \rho_g \psi u_g \sum_{k\in\mathcal{G}} Y_{g,k} h_k\right)\\ &= \frac{1}{r^2}\frac{\partial}{\partial r}\left(r^2 \rho_g \psi D \sum_{k\in\mathcal{G}} \frac{\partial Y_{g,k}}{\partial r} h_k + r^2 \lambda \frac{\partial T}{\partial r}\right).\end{aligned} \tag{20}$$

This balance law is formulated in terms of the total specific enthalpy $h(r,t)$ (in [J/kg]) associated with both phases. With reference to the local volume-averaged particle density $\rho = \rho_g\psi + \rho_s(1-\psi)$, h is defined according to

$$\begin{aligned}\rho h = {}& \rho_g \psi \sum_{k\in\mathcal{G}} Y_{g,k} h_k(T)\\ &+ \rho_s(1-\psi)\sum_{i\in\mathcal{S}} Y_{s,i} h_i(T).\end{aligned} \tag{21}$$

If the intra-particle gas and solid phases conduct heat radially in a parallel fashion, then the thermal conductivity λ in Eq. (20) coincides with the volume average of the conductivities λ_g and λ_s of the two phases,

$$\lambda = \psi\lambda_g + (1-\psi)\lambda_s. \tag{22}$$

In view of the ideal behaviour of the pyrolysis gas and the low Mach number of the intra-particle flow, the gas density ρ_g is linked to the species mass fractions $\mathbf{Y}_g$ and the temperature T by Eq. (2).

Since the flow around the biomass particle is not spatially resolved, we employ a boundary layer treatment to evaluate the rates at which mass and enthalpy are emitted from the particle surface towards the far-field gas. As in the particle's interior, gas phase chemical reactions are neglected. Following the formulation of Spalding [22], the mass and thermal boundary layers coincide ($Le = 1$) and behave in a quasi-steady way [23, Chapters 3 and 10]. For a given boundary layer conductivity $\overline{\rho_g D} = \overline{\mu_g}/Sc$, the conservation laws for the species masses ($k \in \mathcal{G}$) and the gas enthalpy may be integrated analytically across the boundary layer [24, p. 56] to yield the flow rates

$$\dot{m}_{g,k} = 2\pi R \overline{\rho_g D} Sh \left(Y^0_{g,k} - Y^\infty_{g,k}\right), \tag{23}$$

$$\dot{h}_g = 2\pi R \overline{\rho_g D} Nu \left(h^0_g - h^\infty_g\right) \tag{24}$$

in the case $\dot{m}_g = 0$ and

$$\dot{m}_{g,k} = \dot{m}_g \frac{Y^0_{g,k} - Y^\infty_{g,k}\exp\left(-\frac{\dot{m}_g}{2\pi R\overline{\rho_g D} Sh}\right)}{1-\exp\left(-\frac{\dot{m}_g}{2\pi R\overline{\rho_g D} Sh}\right)}, \tag{25}$$

$$\dot{h}_g = \dot{m}_g \frac{h^0_g - h^\infty_g\exp\left(-\frac{\dot{m}_g}{2\pi R\overline{\rho_g D} Nu}\right)}{1-\exp\left(-\frac{\dot{m}_g}{2\pi R\overline{\rho_g D} Nu}\right)} \tag{26}$$

otherwise. The flow rate $\dot{m}_g$ of the gas emanating from the biomass particle, moreover, is computed from

$$\dot{m}_g = 4\pi R^2 \left(\rho_g \psi u_g\right)\Big|_{r=R}. \tag{27}$$

The surface velocity $u_g(R,t)$ that appears here is, in turn, obtained from Eq. (19) and the boundary condition $u_g(0,t) = 0$. In Eqs. (23) to (26), the superscripts 0 and ∞ indicate values at the particle surface and in the far-field, respectively. Note that, for a particle contained in a PaSR with volume $V(t) = \mathrm{vol}\,\Omega(t)$,

the far-field scalars $(\mathbf{Y}_g^\infty, h_g^\infty) = \mathbf{\Phi}(t)$ are random variables that are distributed according to the PDF $f(\cdot, t)$ (Section 3), while $\dot{m}_{g,k}/V(t)$ and $\dot{h}_g/V(t)$ yield the sources $\xi_p(t)\rho_g(\mathbf{\Phi}(t))\dot{s}_k(\mathbf{\Phi}(t), \mathbf{X}_p(t))$ in Eq. (15). Since the Lewis number is unity, the Nußelt and Sherwood numbers Nu and Sh in Eqs. (23) to (26) are equal; they may be evaluated using the Ranz-Marshall correlation [25] which has been calibrated for a particle Reynolds number Re_p in the range $0 \leq Re_p \leq 200$. Following Abramzon and Sirignano [26], the viscosity $\overline{\mu_g}$ across the boundary layer is computed from the surface mass fractions and temperature as well as their far-field counterparts using the 1/3-rule. Because there is no efflux of solid phase enthalpy from the particle, Eqs. (23) through (27) jointly provide the boundary conditions at $r = R$ of Eqs. (18) and (20). At the particle centre, by contrast, symmetry boundary conditions apply.

In order to convert the balance laws in Eqs. (16) to (20) into the form of Eq. (13), we apply a radial finite volume discretisation with staggered variable arrangement. In particular, the degrees of freedom associated with the distributed solid masses $\rho_s Y_{s,i}(1 - \psi)4\pi r^2$, $i \in \mathcal{S}$, the gas' mass fractions $Y_{g,k}$, $k \in \mathcal{G}$, and the temperature T are stored at the cell centres, while the degrees of freedom parameterising the radial intra-particle gas velocity u_g live at the cell faces. Since the radial profile of u_g responds on an instantaneous basis to gas release and temporal changes in the gas density and particle porosity, the semi-discrete counterpart of the mass balance in Eq. (19) yields an algebraic relation that renders the mass matrix $\mathbf{M}$ in Eq. (13) singular.

5. NUMERICAL SOLUTION METHODS

The evolution equation governing $f^\rho(\boldsymbol{\phi}, t)$ (Eq. (15)) corresponds to a differential Chapman-Kolmogorov equation with vanishing diffusion matrix and may, therefore, be associated with a stochastic jump-drift process [27, Chapter 3]. Within the scope of a Monte Carlo solver, different realisations of this process are computed by solving the corresponding SDE for independent random drivers. Since the SDE is kinetically linked to the particles' degrees of freedom $\mathbf{X}_p(t)$ with $p = 1, 2, \ldots$, the deterministic DEM equations (Eq. (13)) are integrated concurrently. Over the course of a time step, the SDE is decomposed into fractional steps using a first order scheme [2, Section 6]. Consequently, physical and chemical effects that occur simultaneously can be treated in a sequential way, thus permitting the application of a dedicated time integration scheme in each fractional step.

6. CONCLUSIONS

In this contribution, we summarised the formal basis of a combined DEM-PaSR model for the pyrolysis of an assembly of spherical biomass particles. Here, the reactive scalars parameterising the gas' thermochemical state are conceived of as random variables whose associated PDF changes in time owing to mass and heat exchanges with the biomass particles, gas phase chemical reactions, micromixing and flow-through. By construction, this statistical description covers small-scale heterogeneity of the gas composition and allows for a closed-form treatment of gas phase chemical reactions. In order to accommodate gas-particle mass and heat exchanges, we argued that the separation of the DEM particles from the bulk gas by a resistive boundary layer permits the approximation of the particle surface-specific joint scalar PDFs in terms of the volume-based PDF that defines the state of the PaSR. Small-scale diffusion and heat conduction, moreover, are accounted for by a micromixing model. The DEM description of a biomass particle is based on a finite volume discretisation of the intra-particle balance laws for the solid species' masses, the masses of the gaseous species, the total gas mass and the combined gas-solid enthalpy. Additionally, the biomass particle is surrounded by a passive boundary layer that restricts the transfer of mass and heat towards the compositionally heterogeneous gas in the far-field.

By design, the PaSR permits a systematic analysis of how large-scale predictables, for example, the pyrolysis duration, the amount of energy consumed and the composition of the pyrolysis gas, are influenced by small-scale heterogeneity in the gas composition. In the near future, we plan to apply the DEM-PaSR model to the pyrolysis of cellulose, the main constituent of woody biomass, and quantify the impact of micromixing limitations.

ACKNOWLEDGEMENTS

This project was funded by the Deutsche Forschungsgemeinschaft (DFG, German Research Foundation) within the scope of the Collaborative Research Centre/Transregio 287 (Project number 422037413).

REFERENCES

[1] O'Brien, E. E., 1980, "The probability density function (pdf) approach to reacting turbulent flows", P. A. Libby, and F. A. Williams (eds.), *Turbulent Reacting Flows*, Springer, Berlin, Heidelberg, Vol. 44 of *Topics in Applied Physics*, pp. 185–218.

[2] Pope, S. B., 1985, "PDF methods for turbulent reactive flows", *Progress in Energy and Combustion Science*, Vol. 11 (2), pp. 119–192.

[3] Haworth, D. C., 2010, "Progress in probability density function methods for turbulent reacting flows", *Progress in Energy and Combustion Science*, Vol. 36 (2), pp. 168–259.

[4] Pope, S. B., 1991, "Computations of turbulent combustion: Progress and challenges", *Symposium (International) on Combustion*, Vol. 23 (1), pp. 591–612.

[5] Chen, J.-Y., 1997, "Stochastic modeling of partially stirred reactors", *Combustion Science and Technology*, Vol. 122 (1–6), pp. 63–94.

[6] Kee, R. J., Rupley, F. M., and Miller, J. A., 1989, "CHEMKIN–II: A FORTRAN chemical kinetics package for the analysis of gas-phase chemical kinetics", *Tech. Rep. SAND89-8009*, Sandia National Laboratories, Livermore, CA.

[7] Poinsot, T., and Veynante, D., 2011, *Theoretical and Numerical Combustion*, Aquaprint, Bordeaux, 3rd edn.

[8] Kee, R. J., Coltrin, M. E., Glarborg, P., and Zhu, H., 2017, *Chemically Reacting Flow: Theory, Modeling, and Simulation*, Wiley, Hoboken, NJ, 2nd edn.

[9] Jones, W. P., and Prasad, V. N., 2010, "Large eddy simulation of the Sandia flame series (D–F) using the Eulerian stochastic field method", *Combustion and Flame*, Vol. 157 (9), pp. 1621–1636.

[10] Anderson, T. B., and Jackson, R., 1967, "A fluid mechanical description of fluidized beds. Equations of motion", *Industrial and Engineering Chemistry Fundamentals*, Vol. 6 (4), pp. 527–539.

[11] Kuo, K. K., 1986, *Principles of Combustion*, Wiley, New York, Chichester.

[12] Capecelatro, J., and Desjardins, O., 2013, "An Euler–Lagrange strategy for simulating particle-laden flows", *Journal of Computational Physics*, Vol. 238, pp. 1–31.

[13] Golshan, S., Sotudeh-Gharebagh, R., Zarghami, R., Mostoufi, N., Blais, B., and Kuipers, J. A. M., 2020, "Review and implementation of CFD-DEM applied to chemical process systems", *Chemical Engineering Science*, Vol. 221, p. 115646.

[14] Mahmoudi, A. H., Hoffmann, F., and Peters, B., 2014, "Detailed numerical modeling of pyrolysis in a heterogeneous packed bed using XDEM", *Journal of Analytical and Applied Pyrolysis*, Vol. 106, pp. 9–20.

[15] Wang, W., Lu, Y., Xu, K., Wu, K., Zhang, Z., and Duan, J., 2021, "Experimental and simulated study on fluidization characteristics of particle shrinkage in a multi-chamber fluidized bed for biomass fast pyrolysis", *Fuel Processing Technology*, Vol. 216, p. 106799.

[16] Lu, L., Gao, X., Shahnam, M., and Rogers, W. A., 2021, "Simulations of biomass pyrolysis using glued-sphere CFD-DEM with 3-D intra-particle models", *Chemical Engineering Journal*, Vol. 419, p. 129564.

[17] Luo, H., Wang, X., Liu, X., Wu, X., Shi, X., and Xiong, Q., 2022, "A review on CFD simulation of biomass pyrolysis in fluidized bed reactors with emphasis on particle-scale models", *Journal of Analytical and Applied Pyrolysis*, Vol. 162, p. 105433.

[18] Crowley, M. F., Sitaraman, H., Klinger, J., Usseglio-Viretta, F., Thornburg, N. E., Brunhart-Lupo, N., Pecha, M. B., Dooley, J. H., Xia, Y., and Ciesielski, P. N., 2022, "Measurement of transport properties of woody biomass feedstock particles before and after pyrolysis by numerical analysis of X-ray tomographic reconstructions", *Frontiers in Energy Research*, Vol. 10, p. 850630.

[19] Papari, S., and Hawboldt, K., 2015, "A review on the pyrolysis of woody biomass to bio-oil: Focus on kinetic models", *Renewable and Sustainable Energy Reviews*, Vol. 52, pp. 1580–1595.

[20] Rabinovich, O. S., Korban, V. V., Pal'chenok, G. I., and Khorol'skaya, O. P., 2009, "Modeling of fast pyrolysis of a single biomass particle in an inert boiling bed", *Journal of Engineering Physics and Thermophysics*, Vol. 82 (4), pp. 611–622.

[21] Finke, J., and Sewerin, F., 2024, "A population balance approach for predicting the size distribution of oxide smoke near a burning aluminum particle", *Combustion and Flame*, Vol. 265, p. 113464.

[22] Spalding, D. B., 1953, "The combustion of liquid fuels", *Symposium (International) on Combustion*, Vol. 4 (1), pp. 847–864.

[23] Turns, S. R., 2012, *An Introduction to Combustion: Concepts and Applications*, McGraw-Hill Series in Mechanical Engineering, McGraw-Hill, New York, 3rd edn.

[24] Williams, F. A., 1985, *Combustion Theory*, Combustion Science and Engineering Series, Addison-Wesley, Reading, Menlo Park, 2nd edn.

[25] Ranz, W. E., and Marshall, W. R., 1952, "Evaporation from drops: Part I", *Chemical Engineering Progress*, Vol. 48 (3), pp. 141–146.

[26] Abramzon, B., and Sirignano, W. A., 1998, "Droplet vaporization model for spray combustion calculations", *AIAA 26th Aerospace Sciences Meeting*, Reno, NV, USA.

[27] Gardiner, C., 2009, *Stochastic Methods: A Handbook for the Natural and Social Sciences*, Springer Series in Synergetics, Springer, Berlin, Heidelberg, 4th edn.